EPJ manuscript No.
(will be inserted by the editor)

On ground-state instability in two-dimensional antiferromagnetic systems

K. Odagiri, T. Yanagisawa

Condensed Matter Physics Group, Electronics Research Institute, National Institute of Advanced Industrial Science and Technology, Tsukuba Central 2, 1–1–1 Umezono, Tsukuba, Ibaraki 305–8568, Japan

January 29, 2014

Abstract. We discuss the stability of the antiferromagnetic ground state in two spatial dimensions. We start with a general analysis, based on Gribov's current-conservation techniques, of the bosonic modes in systems with magnetic order. We argue that the Goldstone ϕ and Higgs h modes mix in antiferromagnetic systems, and this leads to an effective $hh\phi$ three-point interaction. We then analyze the instability of the antiferromagnetic system in two spatial dimensions by studying the non-perturbative behaviour of the Higgs boson self-energy using the Dyson–Schwinger equations. The ground state turns out to be unstable for all values of the three-point coupling. We interpret this as being due to the formation of a (high-T_C) superconducting condensate. The carrier doping dependence of the energy gap has a general behaviour that is consistent with high-T_C superconductivity. Superconductivity co-exists with antiferromagnetic order for large magnetization, or small doping.

PACS. 11.40.-q Currents and their properties – 74.20.-z Theories and models of superconducting state – 74.72.-h Cuprate superconductors – 75.10.-b General theory and models of magnetic ordering

arXiv:1006.4211v1 [cond-mat.supr-con] 22 Jun 2010

1 Introduction

The problem to be discussed in this paper concerns the stability of the antiferromagnetic (AF) ground state, in particular, in two spatial dimensions. This problem is relevant, phenomenologically, to high-T_C superconductivity [1].

Unlike ferromagnetic systems, the movement of electrons in AF systems is subject to non-trivial magnetic interaction which is not well understood, with the notable exception of one spatial dimension. In the one-dimensional case, there is no long-range magnetic order, and spinons and holons are the physical degrees of freedom. This is essentially different from the case of antiferromagnetism in two or more spatial dimensions, where there is long-range magnetic order and the corresponding Goldstone magnons [2] and, because of the high-energy restoration of spin symmetry, Higgs bosons.

We limit our discussion here to two spatial dimensions, not only because of the phenomenological interest, but also because of the relative ease with which the two-dimensional case can be treated. With three spatial dimensions, the short-range interaction, which we would like to treat to all orders, is logarithmically divergent, and at best, in the renormalizable case, something like a renormalization-group equation approach is presumably necessary. Even then, finite-order renormalization-group equations, in general, cannot describe the physical behaviour of a system that develops a condensate, which is the topic of the present investigation.

Our physical picture goes naively as follows.

First, since in the presence of AF order, the movement of single localized electrons disturbs the spin order and therefore costs energy, their movement tends to be in a correlated fashion.

Second, even in this correlated case, the excitation of such spin-singlet pairs generally costs energy, and so the AF ground state is more energetically favourable than the electron-pair state.

Third, in contrast to this usual case, when the correlation becomes strong enough, the creation of spin-correlated pairs becomes so energetically favourable that it costs negative energy to create these pairs. They then condense into a superconducting state.

Given that the electrons cannot be considered to be free, it becomes difficult, and sensitive to the model or formulation, to analyze the electron–electron correlation directly, though we may expect, generally, the following BCS-like [3,4] expression:

$$\Delta_{\mathrm{SC}} \propto e^{-E_e/J}. \tag{1}$$

E_e is some electronic energy scale.

Let us say that the system fundamentally consists of electrons with spin interaction:

$$\mathcal{H} = \mathcal{H}_e, \tag{2}$$

where $\mathcal{H}$ contains the electron field Ψ and its derivatives. We keep the form of $\mathcal{H}_e$ general. We shall make a reference to J later on as the energy required to flip a spin, but only as a means to fix some physical parameters such as the spin-wave velocity.

When the system develops magnetic order, the Goldstone magnons, together with the Higgs boson, become physical de-

grees of freedom:

$$\mathcal{H} = \mathcal{H}_{e'} + \mathcal{H}_{\Phi} + \mathcal{H}_{\rm int}. \tag{3}$$

Here, e' stands for electrons in the presence of magnetic order, and are therefore different from e in eqn. (2). Φ stands for the Goldstone magnons and the Higgs boson collectively, and is, in this sense, like the magnetic order parameter. However, we shall not adopt the order-parameter approach in this paper. $\mathcal{H}_{\rm int}$ stands for the interaction terms between the electrons and Φ.

An important point to keep in mind here is that although the Goldstone bosons and the Higgs boson are fundamentally made of electrons e, they are independent degrees of freedom from e', as the latter stands for electrons moving in a magnetic background. Φ parametrizes the response of the magnetic background. However, the relationship between e' and Φ is severely constrained by the requirement of current conservation (or 'partial conservation'), and we shall make use of this.

Since the AF Higgs boson measures the fluctuations around the AF ground state, studying the Higgs-boson Green's function, in particular its analyticity, is sufficient to discuss the ground-state instability.

Specifically, we consider the corrections to the Higgs boson propagator due to the exchange of Goldstone magnons through a three-point interaction which, we argue, is present in antiferromagnetism because moving electrons in AF background, in general, causes spin waves. The parameters of the theory are fixed in a general way using Gribov's current conservation techniques [5,6], and so our framework is largely model-independent and rely on a minimal set of assumptions. The assumptions are, first, that there is low-energy symmetry breaking and high-energy symmetry restoration; second, the linear spin-wave dispersion relation; and third, that the spin excitation energy is approximately constant in the threshold region.

In order to analyze the non-perturbative behaviour of the theory due to magnon exchange, a non-perturbative framework is necessary. We adopt a Dyson–Schwinger formalism which leads to an ordinary differential equation governing the behaviour of the self-energy as a function of the Higgs–magnon coupling. We then solve this using a factorially divergent perturbative expansion which, in turn, is dealt with by using Borel summation.

This leads to an imaginary part for the Higgs Green's function which has a form similar to eqn. (1), with E_e being given by

$$E_e \propto \hbar^2/M_h a^2, \tag{4}$$

where M_h is the Higgs boson mass and a is the lattice constant.

The calculated mean-magnetization dependence of the energy gap is consistent with the observed doping dependence of the superconducting critical temperature T_C in high-T_C compounds. Our analysis suggests the co-existence of small AF order with superconductivity in the under-doped region.

This paper is organized as follows.

We present a general discussion of spin-current conservation and the bosonic modes in systems with magnetic order in sec. 2. We introduce Goldstone–Higgs mixing in a general way in sec. 3, and this gives rise to an effective Higgs–Higgs–Goldstone vertex.

We evaluate the resulting self-energy correction to the Higgs-boson Green's function. This is worked out, at first, at the one-loop order in sec. 4. The finite part of this calculation is then summed to all orders using the Dyson–Schwinger formalism in sec. 5. We derive a non-linear differential equation, whose solution describes the self-energy correction as a function of the coupling. The power-series solution to this equation has factorially divergent coefficients. We deal with this divergent series using the Borel summation technique in sec. 6.

We make use of the value of the coupling and the mass of the Higgs boson derived in secs. 2, 3 to estimate the magnitude of the superconducting gap in sec. 7. We state our conclusions at the end.

2 General analysis of spin current conservation

In this section, we adapt Gribov's analysis of axial current conservation [5,6] to the context of spin current conservation in systems with magnetic order.

Consider the fermionic (quasi-)electron field which is an $SU(2)_{\rm spin}$ doublet

$$\Psi = \begin{pmatrix} \psi_\uparrow \\ \psi_\downarrow \end{pmatrix}. \tag{5}$$

Let us define the four-vector currents. For Γ^μ defined by the conserved electron current

$$J^\mu_{\rm electron} = \Psi_1^\dagger \Psi_2 \Gamma^\mu, \tag{6}$$

we define 4-vector spin currents J_i^μ ($\mu = 0 \ldots 3$, $i = 1, 2, 3$) of the form

$$J_i^\mu = \Psi_1^\dagger \sigma_i \Psi_2 \Gamma^\mu. \tag{7}$$

For example, J_3^μ is the up-spin current minus down-spin current.

In the spin-symmetric phase, the spin currents are conserved because of the conservation of electrons. That is, the vertex Γ^μ satisfies the Ward–Takahashi identity

$$\Gamma^\mu(q_1 - q_2)_\mu \propto G_1^{-1}(q_1) - G_2^{-1}(q_2). \tag{8}$$

q are 4-vectors.

The Ward–Takahashi identity is violated in the symmetry-broken phase, since there is now an energy difference between the different spin states.

In the ferromagnetic case, we can set locally, and without loss of generality

$$\Psi = \begin{pmatrix} \psi_* \\ \psi \end{pmatrix}. \tag{9}$$

ψ is the spin ground state and ψ^* is the excited state. In the case of antiferromagnetism, we can still denote the spin ground state and the excited state as ψ and ψ^*, respectively. However, in this case, the movement of an electron, in general, disturbs the spin order. We shall discuss this point, in terms of an effective Goldstone–Higgs mixing, in sec. 3.

The energy difference ΔE is given roughly by $\epsilon_* - \epsilon$, and we define it by

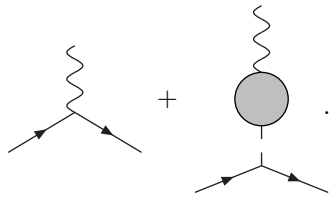
$$\Delta E = G^{-1}(q) - G_*^{-1}(q). \tag{10}$$

ΔE depends on q in principle. In particular, we expect it to vanish far away from the threshold region, that is, $E \approx \epsilon, \epsilon_*$. Furthermore, exactly at the threshold, G^{-1} would, in general, have a singular structure corresponding to the emission and absorption of the Goldstone boson. However, we shall assume it to be roughly constant in the threshold region later on, for the sake of the convenience of parametrization.

With this symmetry violation, the currents $J^{\mu}_{1,2}$ are no longer conserved, and the Ward–Takahashi identity is violated, for constant ΔE, by

$$\Gamma^{\mu}(q_1 - q_2)_{\mu} \propto G_1^{-1}(q_1) - G_2^{-1}(q_2) \pm \Delta E. \qquad (11)$$

This ΔE contribution is of the same form as the coupling of the Goldstone boson ϕ, and current conservation is restored by including the contribution of the Goldstone boson. This is the case even when ΔE is not constant. Specifically, spin current conservation is restored for the vertex modified by the inclusion of the Goldstone boson

$\Gamma =$  (12)

The wavy lines indicate the spin current, and the dashed line indicates the Goldstone boson. The two-point function in the second term is nothing but an electron loop.

The Goldstone boson couples to fermions with strength given by $f^{-1}\Delta E$. We may then deduce the form of the two-point function in eqn. (12), in particular the value of f, by requiring that the Ward–Takahashi identity is restored.

Furthermore, ΔE may be calculated by considering the self-energy correction to the electron propagator due to magnon exchange. The Higgs boson mass M_h, or excitation energy, is evaluated in a similar fashion to the evaluation of f, following ref. [6].

2.1 Case of quadratic dispersion relation

For ferromagnetism, the spin-wave velocity is known to have a quadratic dispersion relation, $\omega \propto k^2$, for small k. In this case, evaluating the electron loop in the two-point function shown in the second term of eqn. (12), between the spin current and the Goldstone boson, yields $f \times (1, \text{const.} \times \mathbf{q})$ in the soft limit, where this constant of proportionality is the same as the constant of proportionality in the dispersion relation. The form factor f has the dimension of (length)$^{-d/2}$.

In the soft limit, we obtain

$$f^2 = -2 \times \int \frac{d^{d+1}k}{(2\pi)^{d+1}i} G(k) G_*(k) \Delta E(k). \qquad (13)$$

The factor 2 is from contracting the Pauli matrices, or for the two spin orientations. By eqn. (10) and the general definition of the Green's function, this is simply the number density

$$f^2 = 2(\rho - \rho_*). \qquad (14)$$

ρ is the number per unit volume or area.

We can define the mean magnetization S, $0 \le S \le 1/2$, by

$$2S/a^d = \rho - \rho_*, \qquad (15)$$

to obtain

$$f^2 = 4S/a^d. \qquad (16)$$

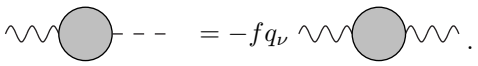
Since $f = 2v$, the vacuum expectation value of a magnetic order-parameter field Φ, this implies $v^2 = S/a^d$, which seems natural. The rotational invariances of Φ correspond to the Goldstone boson(s).

Even though the calculation is ostensibly exact, one may question whether, for instance, eqn. (13) takes into account the higher-order corrections. The corrections to the electron Green's function are included, whereas the vertex corrections are indistinguishable from the self-energy corrections to the Goldstone boson propagator. Our results are therefore exact up to the scale dependence of the form factor. The Goldstone-boson form factor is generally thought to be dependent only (or much more) on the virtuality of the fermions and not on the virtuality of the Goldstone boson [5], and therefore we may consider our results to be exact.

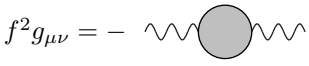
2.2 Case of linear dispersion relation

In the case of a linear dispersion relation for the Goldstone boson as in the AF magnons, it follows that the two-point function shown in the second term of eqn. (12), between the spin current and the Goldstone boson, is given by fq_{μ} (with the spin-wave velocity $u = 1$), where q_{μ} is the 4-momentum. In particular, the two-point function vanishes in the soft limit. In the case of antiferromagnetism, this is due to the cancellation between the two spin orientations, or between the two sub-lattices.

The form factor f^{-1} has the dimension of (energy$\times$length^d)$^{1/2}$. Let us make use of

 (17)

It follows that, for small momenta,

 (18)

For the 0–0 component of this quantity, and for nearly constant ΔE, we obtain

$$f^2 = 2 \times \int \frac{d^d\mathbf{k}}{(2\pi)^d} \frac{1}{\Delta E}. \qquad (19)$$

The factor 2 is again from contracting Pauli matrices. The region of integration covers all points where one spin state is occupied and the other spin state is vacant. In the Neel state, the area of the Fermi surface being given by $(2\pi/a)^d$, we obtain

$$f^2 \approx 2/(a^d \Delta E). \tag{20}$$

Away from the Neel state, let us define the mean magnetization S, $0 \leq S \leq 1/2$, again by

$$2S/a^d = \rho - \rho_*, \tag{21}$$

We then have

$$f^2 = \frac{4S}{a^d \Delta E}. \tag{22}$$

Defining $v = f/2$, we have

$$v^2 = \frac{S}{a^d(\Delta E)}, \tag{23}$$

which is a natural result for the vacuum expectation value of a magnetic condensate.

We may calculate the spin-wave velocity u as the space component of eqn. (18). We obtain

$$f^2 u^2 = 2 \times \int \frac{d^d\mathbf{k}}{(2\pi)^d} \frac{1}{\Delta E} \left(\frac{\partial \epsilon(\mathbf{p})}{\partial \mathrm{p}_i} \right)^2. \tag{24}$$

i.e., u is the root mean squared of the fermion group velocity. We may naively expect it to be of the order of the Fermi velocity, which is higher than expected. On the other hand, we may argue that the fermion group velocity is of the order of the hopping velocity of holes near the insulating state.

2.3 The relationship between f and ΔE

If low-energy dynamics is dominated by magnon exchange, we can calculate ΔE in terms of f and the magnon dispersion relation.

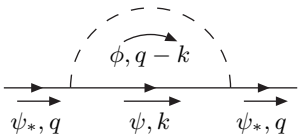


Fig. 1. The electron self-energy diagram.

Corresponding to fig. 1, which is expected to be the main contribution to ΔE, we have

$$\Sigma_*(q) = \int \frac{d^{d+1}k}{(2\pi)^{d+1} i} f^{-2} \Delta E^2 G(k) D(q-k), \tag{25}$$

and similarly for $\Sigma(q)$. D is the Goldstone boson propagator. Following the discussion at the end of sec. 2.1, this result includes all Dyson–Schwinger-type corrections up to the scale dependence of the form factor. It follows that

$$\begin{aligned} &\Sigma_*(q) - \Sigma(q) = \Delta E \\ &= \int \frac{d^{d+1}k}{(2\pi)^{d+1} i} f^{-2} \Delta E^2 \left(G(k) - G_*(k) \right) D(q-k). \end{aligned} \tag{26}$$

The integral contains $G(k) - G_*(k)$ and therefore is proportional to S. We expect $f^{-1}\Delta E$ to vanish away from the threshold region, though we would like to treat both f^{-1} and ΔE to be roughly constant in the threshold region. If the large energy–momentum region does not contribute to ΔE in the threshold region, we can make use of dimensional analysis to estimate ΔE.

In the case of Goldstone bosons ϕ with quadratic dispersion relation corresponding to ferromagnetism, we have $E = \hbar^2 k^2 / 2 m_\phi$. The only dimensional parameters being ΔE and m_ϕ, from dimensional analysis, we expect

$$f^2 \propto S (m_\phi \Delta E / \hbar^2)^{d/2}, \tag{27}$$

with $\mathcal{O}(1)$ coefficient of proportionality. f and ΔE here refer to the relevant quantities in the threshold region. Then using eqn. (16), we have

$$m_\phi \Delta E \propto a^2 \hbar^2, \tag{28}$$

in any number of dimensions. As m_ϕ^{-1} is proportional [7] to JSa^2, this implies that ΔE is proportional to JS. We expect $\Delta E = J$ when $S = 1/2$, and so

$$\Delta E = 2SJ. \tag{29}$$

In the case of Goldstone bosons with linear dispersion relation corresponding to antiferromagnetism, the dimensional parameters are ΔE and u. By dimensional analysis, we obtain

$$f^2 \propto (\Delta E)^{d-1} S / (\hbar u)^d. \tag{30}$$

Again, f and ΔE here mean the relevant quantities in the threshold region. By eqn. (22), we then conclude that

$$\Delta E \propto \hbar u / a, \tag{31}$$

in any number of dimensions. As $\hbar u$ is proportional [7] to JSa, this implies that ΔE is proportional to JS. We expect $\Delta E = J$ in the Neel state, and so

$$\Delta E = 2SJ. \tag{32}$$

This result is the same for both ferromagnetism and antiferromagnetism. In the case of antiferromagnetism, we obtain

$$f^2 = \frac{2}{a^d J}, \tag{33}$$

and therefore the S dependence of f enters, if at all, only through J. It should be noted that J here is defined as the coefficient in the expression for spin-wave velocity. It is not the energy required to flip spin, which is ΔE.

2.4 The Higgs boson

As we expect spin symmetry to be restored in the high energy limit, there is necessarily a Higgs boson h to complement the Goldstone bosons and provide the remaining local rotational degree of freedom. The Higgs boson couples to fermions with the same coupling as the Goldstone bosons, but there is now an energy gap in the zero-momentum limit. This energy gap can be evaluated by the self-energy integral

$$\Sigma_h = \int \frac{d^{d+1}k}{(2\pi)^{d+1}i}(f^{-1}\Delta E)^2 \times [G(k)G(k-q) + G_*(k)G_*(k-q)]\,. \quad (34)$$

Taking the $q \to 0$ limit, and assuming, for simplicity, that $G^{-1}(k) = k_0 - \epsilon(\mathbf{k})$, we then have

$$\Sigma_h = (f^{-1}\Delta E)^2 \lim_{\mathbf{q}\to 0}\int \frac{d^d\mathbf{k}}{(2\pi)^d}\frac{1}{\epsilon(\mathbf{k}) - \epsilon(\mathbf{k}-\mathbf{q})} = (f^{-1}\Delta E)^2 I_h. \quad (35)$$

The integral I_h is some constant or, in general, a function of the direction of $\mathbf{q}$, which depends on the form of $\epsilon(\mathbf{k})$ and on the number of dimensions. Since, in the zero-momentum limit, only the region close to the (spin-asymmetric) Fermi surface contribute to the integral, we see that I_h is equivalent to the surface integral

$$I_h = (2\pi)^{-d}\int_{\mathbf{q}\cdot\mathbf{v}>0}\frac{\mathbf{q}\cdot d\mathbf{S}_\mathbf{k}}{\mathbf{q}\cdot\mathbf{v}(\mathbf{k})} \equiv (2\pi)^{-d}\int_{\mathbf{q}\cdot\mathbf{v}>0}\frac{|d\mathbf{S}_\mathbf{k}|}{|\mathbf{v}(\mathbf{k})|}. \quad (36)$$

$\mathbf{v}(\mathbf{k})$ is the group velocity. If $|\mathbf{v}(\mathbf{k})|$ is constant over the (Fermi) surface, I_h is simply a half of the carrier density per unit energy range, $g_F = g(E_F)$, so that

$$\Sigma_h = \frac{g_F}{2}(f^{-1}\Delta E)^2. \quad (37)$$

In ferromagnetism, the self-energy gives the excitation energy E_h of the Higgs boson. By eqns. (16, 29), we obtain

$$E_h = \frac{J^2 S a^d g_F}{2}. \quad (38)$$

In antiferromagnetism, the self-energy corresponds to $(M_h u^2)^2$, where M_h is the Klein–Gordon mass of the Higgs boson and u is the spin-wave velocity. The excitation energy is given by $M_h u^2$. Using eqns. (32, 33), we obtain

$$(M_h u^2)^2 = J^3 S^2 a^d g_F. \quad (39)$$

Thus the excitation energy falls as S in both cases. The AF case is suppressed less by $Ja^d g_F$ than the ferromagnetic case.

3 Higgs–Goldstone coupling

In the AF state, moving an electron to its neighbouring site, without disturbing the AF order, requires flipping the spin of the electron. This takes place via the emission of a magnon. However, moving the electron without raising it to the spin-excited state corresponds to the Higgs boson, and so the Higgs boson couples to the Goldstone boson, or there is effectively a mixing between the Higgs boson and the magnon.

At the moment, we do not know how to calculate this mixing. It is certainly possible to estimate it in a number of ways from the consideration of the form of the AF ground state, but let us keep the discussion general here by parametrizing the mixing by a single mixing angle $\theta_{h\phi}$, or simply θ. θ can also be thought of as a mixing angle between ψ on one sub-lattice and ψ_* on the other.

We denote the mixed states h' and ϕ' as

$$\begin{pmatrix} h' \\ i\phi' \end{pmatrix} = \begin{pmatrix} \cos\theta & \sin\theta \\ -\sin\theta & \cos\theta \end{pmatrix}\begin{pmatrix} h \\ i\phi \end{pmatrix}. \quad (40)$$

These mixed states are the physical states, and the assumption is that $M_{h'}u^2$ is the same as $M_h u^2$ calculated in the previous section, and $M_{\phi'}$ is zero. We can easily show that this is the case if the h–ϕ mixing occurs, via the electron loop, from the mixing of ψ and ψ_*.

So long as the ϕ–h mixing is due to the mixing of ψ and ψ_*, there is no loop-induced contribution to the three-point function.

In general, only one linear combination of Goldstone bosons is involved, and the other Goldstone boson mode remains orthogonal to both h' and ϕ'.

In terms of h and ϕ, the $h\phi\phi$ coupling is given by

$$\frac{\hbar^2}{2}vh(f^{-1}\partial_\mu\phi_2)^2. \quad (41)$$

This arises generally from the transformation property of h and ϕ, as can be seen from the kinetic-energy part of the effective Lagrangian for the order parameter field

$$\mathcal{L}_{\text{kinetic}} = \frac{\hbar^2}{2}(\partial_\mu\Phi_i)^2 = \frac{\hbar^2}{2}\left[\left(\frac{\partial\Phi_i}{\partial t}\right)^2 - u^2\left(\nabla\Phi_i\right)^2\right]. \quad (42)$$

$v = f/2$ as before.

We are interested in the $\phi' h' h'$ coupling. From eqn. (41), for near on-shell Higgs bosons, and in terms of h' and ϕ', the three-point coupling Γ is found to be given by

$$\frac{\Gamma}{2!} \approx \frac{\hbar^2 f^{-1}(M_{h'}u^2)^2}{4}\sin\theta(1 - 3\cos^2\theta). \quad (43)$$

The 2! is the identical particle factor. Even though there is, in principle, a four-point function in addition to the three-point interaction, we do not know how to sum both three-point and four-point vertices to all orders, and therefore we adopt the approximation of eqn. (43).

For the sake of later analysis, let us introduce the dimensionless coupling x, defined by

$$x = \frac{-\Gamma^2}{4\pi M_{h'}^3 u^6} \times \frac{1}{(\hbar u)^2}. \quad (44)$$

This is then given by

$$x \approx -\frac{f^{-2}M_{h'}u^2}{16\pi(\hbar u)^2}\sin^2\theta(1-3\cos^2\theta)^2 = -\frac{JM_{h'}u^2}{32\pi(\hbar u/a)^2}\sin^2\theta(1-3\cos^2\theta)^2. \quad (45)$$

In two spatial dimensions, from ref. [8], $\hbar u$ is found to be

$$\hbar u = c_2 JSa \approx 5.47JSa. \quad (46)$$

c_2 means the coefficient in two spatial dimensions. Therefore

$$x \approx -\mathcal{O}(10^{-4}) \times \frac{M_{h'}u^2}{JS^2}. \quad (47)$$

This is somewhat surprising in the sense that it implies that the dimensionless coupling x grows as the magnetization falls. However, this behaviour is correct, as we shall show later, since this leads to the survival of magnetic order in the large-magnetization region.

4 One-loop results

Our objective is to analyze vacuum instability due to the exchange of Goldstone magnons. In two spatial dimensions and in the leading-order approximation, the potential due to the single exchange of a magnon is proportional to $\log(r)$ in the real space. The potential is therefore unbound as r goes to infinity. This makes Higgs pairs long-distance, or infra-red, confined. However, confinement does not make the Higgs pair state more energetically favourable than the AF ground state. That requires Higgs-pair super-criticality, which is an $\mathcal{O}(\hbar/M_{h'}u)$ short-distance effect.

Furthermore, Higgs-pair super-criticality is not necessary for electron-pair condensation, although the latter affects the analyticity of the Higgs-boson Green's function.

In two spatial dimensions, we have strong infra-red divergence which we are unable to treat to all orders, and finite ultraviolet contributions which can be summed to all orders as we shall discuss. We sum the finite terms because super-criticality is a short-distance effect and so we consider this treatment to be sufficient. In this regard, we should note that the superconducting coherence length is indeed relatively short in the real high-T_C systems [1], which adds support to our discussion.

Let us start with the one-loop self-energy correction to the Higgs boson propagator. The corresponding Feynman diagram is shown in fig. 2. All momenta are $2+1$-vectors, i.e., with two space and one time components.

In the following, let us adopt the convention $\hbar = u = 1$. It is easy to reintroduce them by counting the dimensions. Using the scheme developed in the preceding section, the one-loop self-energy $\Sigma_1(q)$ is given by

$$\Sigma_1(q) = \Lambda_0 \int \frac{d^3k}{(2\pi)^3 i}\frac{1}{(q-k)^2+i\delta}\frac{1}{k^2-M_0^2+i\delta}. \quad (48)$$

M_0 is the bare mass for the Higgs boson, and is the same quantity as that denoted as $M_{h'}$ in the previous section. The change in the notation is so as to be more clear when discussing the mass renormalization. Λ_0 is minus the coupling constant squared which, according to eqn. (43), is given by

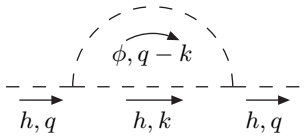


Fig. 2. The one-loop self-energy diagram.

$$\Lambda_0 = -f^{-2}(M_0u^2)^4. \quad (49)$$

The subscript 0 indicates that it is the bare coupling, to which we shall calculate the corrections which arise due to the vertex correction diagrams (and not due to the vacuum polarization diagrams). We have included the factor 2 for the two Goldstone modes. As explained below eqn. (43), the factor 2 for identical Higgs bosons has already been taken into account. The choice of the sign is such that positive Λ_0 corresponds to repulsion and negative Λ_0 to attraction. Λ_0 has the dimension $(\text{energy})^5 \times \text{area}$.

Eqn. (48) can be integrated easily using standard methods [9]. First, the usual procedure of combining the denominators yields

$$\Sigma_1(q) = \Lambda_0 \int_0^1 d\lambda \int \frac{d^3\ell}{(2\pi)^3 i} \left[\ell^2 + \lambda\left(q^2(1-\lambda) - M_0^2\right) + i\delta\right]^{-2}. \quad (50)$$

The Wick rotation yields

$$\Sigma_1(q) = \Lambda_0 \int_0^1 d\lambda \int \frac{d^3\tilde{\ell}}{(2\pi)^3} \left[-\tilde{\ell}^2 + \lambda\left(q^2(1-\lambda) - M_0^2\right) + i\delta\right]^{-2}. \quad (51)$$

Evaluating this Euclidean integral, we obtain

$$\Sigma_1(q) = \frac{\Lambda_0}{8\pi}\int_0^1 d\lambda \left[\lambda\left(M_0^2 - q^2(1-\lambda)\right) - i\delta\right]^{-1/2}. \quad (52)$$

Finally, under the condition $M_0^2 > q^2 > 0$, we obtain

$$\Sigma_1(q) = \frac{\Lambda_0}{4\pi\,|q|}\tanh^{-1}\frac{|q|}{M_0}, \quad (53)$$

where $|q| = \sqrt{q^2}$. Near $|q| = M_0$, this diverges logarithmically, reflecting the long-distance confinement. In the region $|q| < M_0$, Σ has the following expansion:

$$\Sigma_1 \approx \frac{\Lambda_0}{4\pi M_0^3}\left(M_0^2 + \frac{q^2}{3} + \frac{q^4}{5M_0^2} + \cdots\right). \quad (54)$$

Let us retain the first two terms. This approximation is accurate to 10% up to $|q|/M_0 = 0.7$ or so.

Since we have the following general relation:

$$G^{-1} = Z^{-1}(q^2 - M^2) = q^2 - M_0^2 - \Sigma, \qquad (55)$$

we can immediately write down the one-loop Z and M^2 as

$$Z_1^{-1} = 1 - \frac{\Lambda_0}{12\pi M_0^3}, \qquad \frac{M_1^2}{M_0^2} = Z_1\left(1 + \frac{\Lambda_0}{4\pi M_0^3}\right). \quad (56)$$

This corresponds to a (short-distance) correction to the Higgs-boson mass of the form

$$M_1^2 = M_0^2 - \Sigma_1 \approx M_0^2 + \frac{\Lambda_0}{4\pi M_0} = M_0^2(1 + x). \qquad (57)$$

The dimensionless coupling x is defined in eqn.(44).

For the sake of completeness, it is relatively easy to extend the preceding analysis to the case with an artificial small mass m for the (pseudo-)Goldstone boson, which screens the interaction with a characteristic distance $\hbar/mu$. In this case, the one-loop self-energy correction is given by

$$\Sigma_1 = \frac{\Lambda_0}{4\pi\,|q|}\tanh^{-1}\frac{|q|}{M_0 + m} \qquad (58)$$

We again see that the self-energy diverges near the threshold, corresponding to the long-distance correction mediated by the Goldstone boson which goes almost on shell.

Let us now consider the vertex correction.

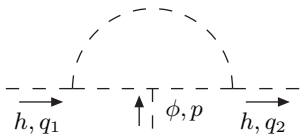


Fig. 3. The one-loop vertex-correction diagram.

The one-loop amplitude is given by

$$\Gamma_1/\Gamma_0 - 1 = \Lambda_0 \int \frac{d^3k}{(2\pi)^3 i}\frac{1}{k^2 + i\delta} \times \frac{1}{(q_1 - k)^2 - M_0^2 + i\delta}\frac{1}{(q_2 - k)^2 - M_0^2 + i\delta}. \quad (59)$$

$\Gamma_0 = 1$ in our normalization convention. Γ_1 is Γ_0 plus the the one-loop correction. Proceeding in a similar fashion to that for the self-energy, we obtain the following Feynman parameter integral:

$$\Gamma_1/\Gamma_0 - 1 = \frac{\Lambda_0}{32\pi}\int_0^1 d\lambda_1 d\lambda_2 d\lambda_3 \delta(1 - \sum_{i=1}^{3}\lambda_i) \big[\big(\lambda_1 M_0^2 - q_1^2\lambda_2\lambda_3\big) + \big(\lambda_2 M_0^2 - q_2^2\lambda_1\lambda_3\big) - p^2\lambda_1\lambda_2 - i\delta\big]^{-3/2}. \quad (60)$$

In the general case, eqn. (60) is difficult to handle analytically, even though the first two integrations are relatively easy. We have nevertheless been able to evaluate it with the aid of the on-line software [10] based on MATHEMATICA, but the result is cumbersome and so we do not reproduce it here.

Here let us consider the limit in which the exchange momentum p is small compared with the other scales involved. In other words, we make the approximation

$$\Gamma(q_1, q_2, p) \approx \Gamma(q, q, 0), \qquad (61)$$

where $q \approx q_1, q_2$. There is a physical basis to this approximation, namely that we expect the interaction of the Goldstone boson to depend only on the virtuality of the interacting particles and not the Goldstone boson itself [5]. For the same reason, we expect the vacuum polarization contribution to the Goldstone boson to be small. At the very least, such contributions are not allowed to make the excitation energy of Goldstone modes finite and thus violate the Goldstone theorem.

In this limit of small p, the vertex-correction amplitude is related to the self-energy amplitude by

$$\Gamma_1/\Gamma_0 - 1 = \frac{\partial\Sigma_1}{\partial M_0^2}. \qquad (62)$$

This can be deduced from the form of eqn. (48). Taking $q^2 \ll M_0$, the application of eqn. (62) to the leading term of eqn. (54) yields

$$\Gamma_1/\Gamma_0 - 1 \approx -\frac{\Lambda_0}{8\pi M_0^3}. \qquad (63)$$

From eqn. (56), the one-loop estimate for the critical coupling is $-\Lambda_0 \approx 4\pi M_0^3$, at which point the one-loop mass becomes zero, and above which the mass becomes tachyonic. At this value of $-\Lambda_0$, by eqn. (63), the one-loop vertex correction makes the effective vertex greater by 50%. Clearly, finite-order calculations are insufficient to deal with such corrections and so a non-perturbative method is needed. In the next section, we shall sum such contributions to all orders using the Dyson–Schwinger equations.

Before proceeding, we note that a tachyonic Higgs mass by itself only suggests the instability of the AF ground state, and not the form of the true ground state. For instance, one may very well conclude at this stage that the true ground state is given simply by $v = 0$, i.e., zero magnetization, which would be a reasonable interpretation for tachyonic Higgs mass. We shall show, however, that this is only partially true. In the all-order analysis, the real part of the Higgs-mass squared does indeed go negative above a certain value of the coupling, but ground-state instability occurs regardless of the sign of the real part of the Higgs-mass squared.

5 Dyson–Schwinger equations

We have shown that finite-order treatment is insufficient. In particular, we would like to sum the finite short-distance contributions to all orders. Let us deal with this problem by making use of the Dyson–Schwinger equations.

First, the self-energy contribution is shown diagrammatically in fig. 4. It can be seen that this includes all possible perturbative corrections that involve the $hh\phi$ coupling, other than

vacuum polarization. The non-perturbative equation is thus a modification of eqn. (54), given by

$$\Sigma = (q^2 - M_0^2) - Z^{-1}(q^2 - M^2) = \frac{\Gamma\Gamma_0}{4\pi M^3}\left(M^2 + \frac{q^2}{3} + \cdots\right). \quad (64)$$

M, Σ and Γ are now all-order quantities. We have, for the sake of simplicity of notation, absorbed Λ_0 in the definition of Γ. That is, $\Gamma_0 = \sqrt{\Lambda_0}$, and Γ also includes the factor $\sqrt{\Lambda_0}$. Eqn. (64) sums only the finite terms in the higher-order corrections, and not the singular infra-red contributions.

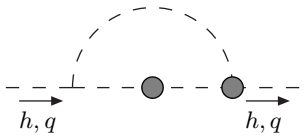


Fig. 4. The self-energy diagram corresponding to the Dyson–Schwinger equation. The blobs represent corrections to all orders.

Let us introduce the following notation:

$$y = \frac{M}{M_0}, \qquad w = \frac{\Sigma(q=0)}{M_0^2}, \qquad g = \frac{\Gamma}{\Gamma_0}. \quad (65)$$

y is the normalized mass, which we would like to obtain as a function of the normalized coupling x defined by eqn. (44). w is the normalized self-energy and g gives the coupling renormalization. From eqn. (64), we derive the following:

$$w = y^2 Z^{-1} - 1 = \frac{3}{4}(y^2 - 1), \qquad xyg = w(w+1). \quad (66)$$

As for the vertex correction, we can write it as the sum of two diagrams, as shown in fig. 5.

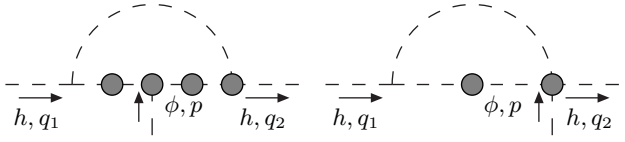


Fig. 5. The two diagrams whose sum contains all of the vertex-correction contributions.

The second of these diagrams contains a 4-point vertex, and it would ordinarily be necessary to construct another Dyson–Schwinger equation to describe it. However, as we saw in the previous chapter, so long as we are allowed to approximate the vertex by a 0-momentum vertex, the insertion of a Goldstone-boson vertex is formally equivalent to the derivative by M_0^2 and multiplication by Γ_0. That is, the sum of the two diagrams in fig. 5 is given simply by

$$\Gamma/\Gamma_0 - 1 = \frac{\partial\Sigma}{\partial M_0^2} \quad (67)$$

The partial derivative means differentiating by M_0^2 while keeping Λ_0 constant. Now Σ is a function of both Λ_0 and M_0^2, but by counting the dimensions, Σ is of the form

$$\Sigma = M_0^2 w(x), \quad (68)$$

where x is as defined by eqn. (44). Thus eqn. (67) can be written as

$$g = 1 + w - \frac{3x}{2}\frac{dw}{dx}. \quad (69)$$

To proceed, we make use of eqn. (66) to eliminate g from eqn. (69). This yields the following ordinary, first-order and non-linear differential equation:

$$\frac{3x}{2}\frac{dw}{dx} = (1+w)\left(1 - \frac{w}{xy}\right). \quad (70)$$

In order to obtain $w = (3/4)(y^2 - 1)$ as a function of x, we then need to solve eqn. (70) with the boundary condition

$$w(0) = 0. \quad (71)$$

Unfortunately, this boundary condition makes the solution to eqn. (70) difficult. We do not think that eqn. (70) can be integrated analytically and, on the other hand, numerical implementation suffers from instability near $x = 0$ where eqn. (70) contains $0/0$.

Let us adopt a power-series solution. Simply expanding y in powers of x and substituting in eqn. (70), we are able to read off the coefficients with the boundary condition given by eqn. (71). To simplify this otherwise tedious task, we made use of MAXIMA [11] for preliminary algebra and the evaluation of the first 28 coefficients, and FORM [12] after that. Using FORM, we calculated the first 102 coefficients, which, in our implementation, is equivalent to having verified the first 101. On a LINUX machine equipped with a 2.6 GHz Pentium 4 processor, the evaluation of the last coefficient took just over 5 minutes to perform. The machine has 2 GB memory, but less than 1 % of the memory was taken up by the calculation. The first few are given by

$$y = 1 + \frac{2}{3}x - \frac{7}{9}x^2 + 2x^3 - \frac{641}{81}x^4 + \frac{2321}{54}x^5 - \mathcal{O}(x^6). \quad (72)$$

It should be noted that x being the normalized coupling, the expansion in x should match with the finite terms from the perturbative calculation, order by order. For example, the truncation of eqn. (72) at the first order in x reproduces the one-loop perturbative result, eqn. (56), at the first power order in Λ_0.

This series is divergent for all non-zero x, i.e., the critical coupling x_c, which is calculated as

$$x_c = \lim_{n\to\infty} \frac{a_{n-1}}{a_n}, \quad (73)$$

vanishes. Here, a_n stands for the coefficient of the n'th power of x. The radius of convergence of the series is given by $|x_c|$.

We plot the ratio appearing in eq. 73, for finite n, with n up to 10 in fig. 6. We have found that these are numerically consistent with

$$\frac{a_{n-1}}{a_n} = \left[\frac{11}{6} - \frac{3n}{2} + \mathcal{O}(n^{-1})\right]^{-1}. \quad (74)$$

The coefficient of the $\mathcal{O}(n^{-1})$ contribution is about 0.3, numerically. We see that for large n, the series is factorially divergent, and the radius of convergence is therefore zero.

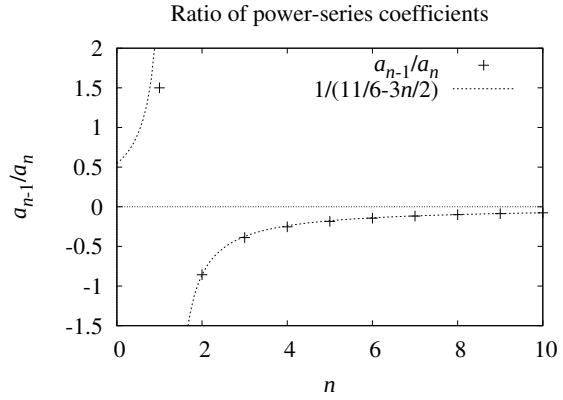


Fig. 6. The ratio a_{n-1}/a_n, for $1 \leq n \leq 10$, compared with the expression $(11/6 - 3n/2)^{-1}$.

6 Borel summation

A method which is commonly used to assign a meaning to factorially divergent expansions is that of Borel summation. For $Y(X)$ given by the power series

$$Y(X) = \sum_{n=0}^{\infty} A_n X^{-n}, \tag{75}$$

the Borel transformed series is given by

$$\mathcal{B}Y(t) = \sum_{n=0}^{\infty} \frac{A_{n+1}}{n!} t^n. \tag{76}$$

$Y(X)$ is then recovered by the Laplace transform

$$Y(X) = A_0 + \int_0^{\infty} \mathcal{B}Y(t) e^{-Xt} dt. \tag{77}$$

Since eqn. (77) requires $X > 0$, let us define

$$X = 1/x, \quad A_n = a_n, \quad y(x) = Y(1/x), \tag{78}$$

when $x > 0$, and

$$X = -1/x, \quad A_n = (-1)^{n+1} a_n, \quad y(x) = -Y(-1/x), \tag{79}$$

when $x < 0$. We can then readily find the Borel transformed series $\mathcal{B}Y(t)$.

Alternatively, using the first two terms of eqn. (74), we can estimate the Borel sum to be

$$\begin{aligned} \mathcal{B}Y(t) &\approx a_1(1 + 3t/2)^{-7/9} \qquad (x > 0), \\ \mathcal{B}Y(t) &\approx a_1(1 - 3t/2)^{-7/9} \qquad (x < 0). \end{aligned} \tag{80}$$

In fig. 7, we compare this estimation, with $a_1 = 2/3$, against the series expansion using the actual values of a_n up to a_{100}. For the range of $\mathcal{B}Y(t)$ shown in fig. 7, the contribution of the last term in the expansion is at most about 0.5% of the total number, and therefore we consider the error due to the truncation of the power series to be negligible. The two expressions match reasonably well. We shall henceforth make use of the estimation of eqns. (80) in our discussions.

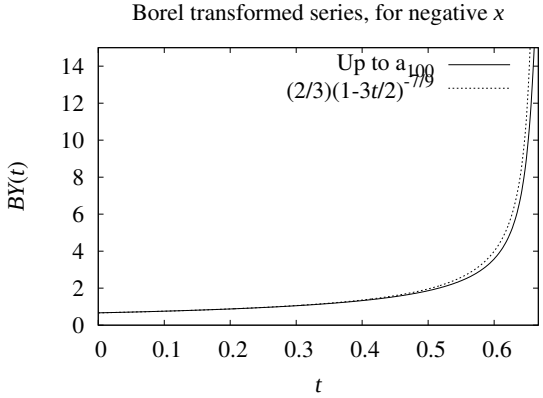


Fig. 7. $\mathcal{B}Y(t)$ for negative x, using the calculated a_n ($n \leq 27$), and the estimation $a_n \approx b_n$.

For positive x, eqn. (80) has a unique Laplace transform. In other words, the series is Borel summable. The result of the Laplace transform is

$$y(x) = a_0 + a_1(2/3)^{7/9} e^{2/3x} x^{2/9} \Gamma(2/9, 2/3x) \qquad (x > 0), \tag{81}$$

again using the approximation of taking the first two terms of eqn. (74). Γ is the upper incomplete Gamma function, defined by

$$\Gamma(s, a) = \int_a^{\infty} t^{s-1} e^{-t} dt. \tag{82}$$

On the other hand, for negative x, eqn. (80) has a branch-point singularity at $t = 2/3$. In other words, the series is non-Borel summable. We can still derive the expression for $y(x)$ formally, and the result turns out to be of the same form as eqn. (81), but it is dependent on the choice of the contour of integration. The perturbation series is thus ambiguous. However, in our case, we simply choose the contour such that we obtain a negative imaginary part for the self-energy, corresponding to the retarded Green's function. This choice of the contour is obtained by moving the singularity downwards in the complex t plane, as shown in fig. 8.

This is equivalent to giving a negative and infinitesimal imaginary part to x, and so in the end, we have, for both positive and negative x, as well as $x = 0$,

$$y(x) = 1 + \frac{4}{9} \exp\left(\frac{2/3}{x - i\delta}\right) \left(\frac{2/3}{x - i\delta}\right)^{-2/9} \Gamma\left(\frac{2}{9}, \frac{2/3}{x - i\delta}\right). \tag{83}$$

The definition of the incomplete Gamma function, as given by eqn. (82), is ambiguous for negative or complex a. A more gen-

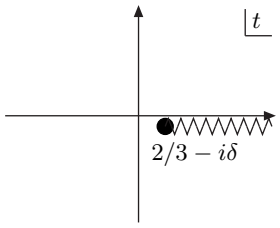


Fig. 8. Moving the branch cut off the real axis. The contour of integration is along the positive real axis.

eral formula reads

$$\Gamma(s,z) = \Gamma(s) - \gamma(s,z) = \Gamma(s) - \sum_{k=0}^{\infty} \frac{(-1)^k}{k!} \frac{z^{s+k}}{s+k}, \quad (84)$$

using which we are able to evaluate $y(x)$ numerically. $\gamma(s,z)$ is the lower incomplete Gamma function. The resulting form of $y(x)$, and $y^2(x)$, is shown in fig. 9.

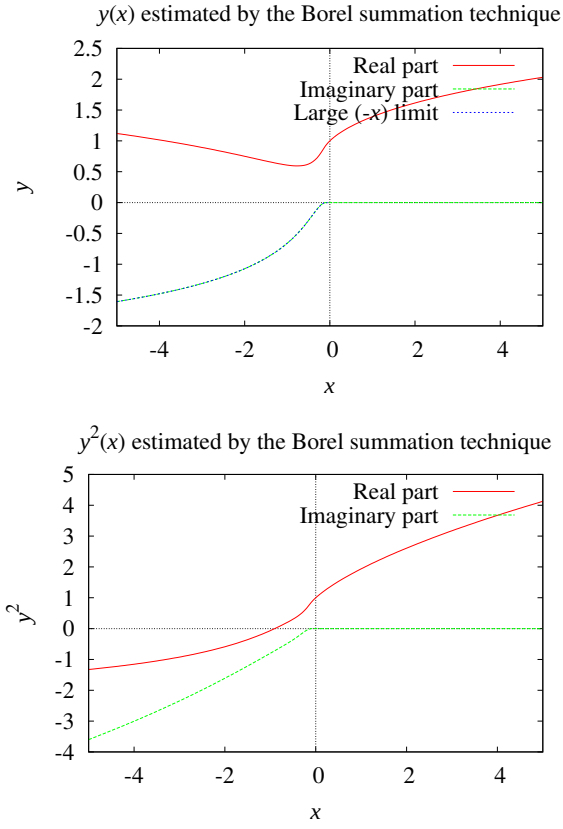


Fig. 9. $y(x)$ (upper figure), and $y^2(x)$ (lower figure), evaluated as the Laplace transform of eqn. (80).

In fig. 9, we also show the function

$$-(4/9)\Gamma(2/9)\sin(2\pi/9)e^{2/3x}(-2/3x)^{-2/9}, \quad (85)$$

for negative x. This is an $x \to -\infty$ limit of the imaginary part of eqn. (83), and it agrees well with the imaginary part of $y(x)$.

In general, we expect that any singularity at $t = t_0$ in the Borel transform induces a term of the form $e^{t_0/x}$. Since the imaginary part of the Green's function corresponds to the binding energy of the condensate, this implies a BCS behaviour of the energy gap. There is nothing new in this particular behaviour of the perturbation series, the so-called renormalon [13] being a celebrated example.

We note that, unlike in finite-order calculations, the criticality, in the sense of an imaginary part for y, develops already at $x = -0$, even though it is quite small until $-x$ becomes comparable with $2/3$. The criticality indicates the decay to a bosonic condensate which, when expressed in terms of the electrons, can only be a superconducting condensate.

The real part of y remains positive, and this is against our naive expectation that strong attractive interaction makes the single-particle mass negative. There is a balance between the attractive interaction mediated by the Goldstone boson and the contribution due to the condensate which counteracts it. The former is dominant at small $-x$, and the latter is dominant at large $-x$.

The real part of y^2 becomes negative at $x \approx -0.9$. Naively speaking, AF order co-exists with the new condensate state for $x \gtrsim -0.9$, and is destroyed below this value of x.

7 Phenomenological discussions

In the preceding sections, we were able to deduce the non-perturbative behaviour of the single-particle Green's function for the Higgs boson.

As per conventional wisdom [4], the imaginary part of the self-energy determines the relaxation time of the unstable ground state which, in turn, and by the uncertainty principle, is the inverse of the binding energy.

The energy gap is thus given simply by

$$2\Delta = -\mathrm{Im}\, M \equiv -M_0 u^2 \mathrm{Im}\, y, \quad (86)$$

and therefore has a BCS-like behaviour. It should be noted that although 2Δ is indeed the energy gap between the superconducting ground state and the AF ground state, this amount of energy is not sufficient to excite Higgs-boson pairs, because doing so requires a further energy of $2\mathrm{Re}Mu^2$.

The total condensation energy, per unit area, is given by the two-dimensional phase-space integral

$$\frac{E_{\mathrm{cond}}}{A} = -\int \frac{d^2\mathbf{k}}{(2\pi)^2} \mathrm{Im}\sqrt{\mathbf{k}^2 + M^2} = -\frac{1}{6\pi}\mathrm{Im}\left((K^2+M^2)^{3/2} - M^3\right). \quad (87)$$

K stands for the upper limit of integration, which is close to π/a. Taking the limit as the K tends to infinity, the binomial expansion of eqn. (87) yields

$$\frac{E_{\mathrm{cond}}}{A} = -\frac{1}{4\pi} K \mathrm{Im}\, M^2. \quad (88)$$

This expression, for very large $-x$, has the behaviour $(-x)^{4/9}$, or proportional to Δ^2.

It is more difficult to calculate T_C, even though, physically, we expect that this critical temperature is proportional to the energy gap, which is given by eqn. (86).

Let us define S_0 by

$$-2/3x = S/S_0. \tag{89}$$

Then we obtain, by eqn. (45),

$$S_0 = \frac{3}{\pi}\left(\frac{\sin\theta(1-3\cos^2\theta)}{8c_2}\right)^2 \sqrt{Ja^2g_F} = c_S\sqrt{Ja^2g_F}. \tag{90}$$

The coefficient c_S satisfies $0 \le c_S \le 3/64\pi c_2^2$ and is of order 10^{-3}. c_S can depend on S through θ. We also obtain

$$M_0u^2 = (S/S_0) \times c_S J^2a^2g_F. \tag{91}$$

Using eqn. (85), the superconducting gap is then estimated as

$$2\Delta_{\rm SC} = 1.17c_S J^2a^2g_F e^{-S/S_0}(S/S_0)^{7/9}. \tag{92}$$

This is shown in fig. 10. For large S, the exponential factor tends to suppress superconductivity, whereas for small S, the M_0u^2 factor suppresses it. The maximum of $2\Delta_{\rm SC}$ as a function of S/S_0 occurs at $S/S_0 = 7/9$.

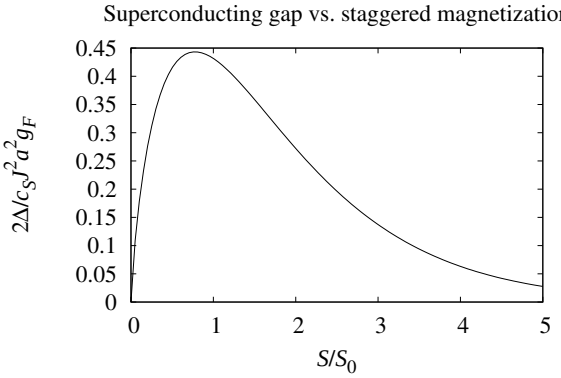


Fig. 10. The superconducting gap, normalized to $c_S J^2a^2g_F$, as a function of the mean staggered magnetization S normalized to S_0.

Small S and large S correspond to over-doping and under-doping, respectively, and therefore the general behaviour is consistent with the doping behaviour of high-T_C superconductors. From eqns. (90, 92), we see that the measurement of S_0, through the measurement of the magnetization at the peak of $2\Delta_{\rm SC}$ or otherwise, together with the measurement of, say, g_F and a, constrains $2\Delta_{\rm SC}$ within a certain range, up to the value of c_S. This is then a prediction of our calculation.

In the sense of the positivity of the real part of the renormalized $M^2 = M_0^2y^2$, superconductivity co-exists with antiferromagnetism down to about $x = -0.90$, or $S/S_0 = 0.74$ ($0.74 < 7/9 = 0.77\cdots$). Antiferromagnetism disappears in the over-doping region.

As for the overall magnitude of $\Delta_{\rm SC}$, an $\mathcal{O}(100\ \mathrm{meV})$ superconducting gap is obtained when $J^2a^2g_F$ is $\mathcal{O}(100\ \mathrm{eV})$. For J of the order of 0.1 eV, we therefore require a^2g_F to be of the order of $(0.1\ \mathrm{meV})^{-1}$, leading to $S_0 \sim 10^{-2}$. This large value of g_F presumably requires the presence of a Van Hove singularity. The situation is improved for greater values of J or c_S.

As discussed below eqn. (24), our calculation seems to indicate that the spin-wave velocity is of the order of the electron group velocity. On the other hand, g_F is proportional to the inverse of the electron group velocity. Therefore there may be a cancellation between these contributions. However, as we mentioned below eqn. (24), this estimate of the spin-wave velocity being apparently much greater than is expected, we would like to leave this point as it is.

As for the symmetry of the superconducting gap, our analysis does not single out a particular type of symmetry, but we expect, naively, that the requirement of forming spin-singlet pairs in AF background restricts pair formation in the $(\pm\pi, \pm\pi)$ directions, and so there are necessarily nodes in those directions.

8 Conclusions

We made an adaptation of Gribov's current conservation techniques to the situation of spin-current conservation in systems with magnetic order. We obtained the coupling strength of the Goldstone bosons, and the mass of the Higgs boson in a non-perturbative manner. Our analysis is general, and does not depend on a particular formulation of the electron or the interaction Hamiltonian.

In AF systems, due to the spin interaction experienced when moving an electron to its neighbouring sites, we expect there to be a mixing between the Goldstone and Higgs modes. This gives rise to an effective Higgs–Higgs–Goldstone three-point interaction.

We then discussed the stability of the AF ground state with respect to the collapse due to this interaction, which is attractive. In view of the observation of high-T_C superconductivity in two-dimensional AF systems, we restricted our discussion to the two-dimensional case, which is easier in the sense that the short-distance integral converges.

The exchange of Goldstone magnons induces non-analyticity in the Higgs-boson Green's function. This implies that the AF ground state is unstable at low temperature. The analysis of the Higgs-boson Green's function was carried out in an all-order manner, by using a Dyson–Schwinger summation of the relevant finite, short-distance, contribution to all orders. We found a solution for the mass renormalization as a power series in the coupling constant. The power series is factorially divergent, but can be treated using the Borel summation method.

We found that an essential singularity develops in the mass renormalization when the coupling constant is zero. We thus conclude that the true AF ground state in two spatial dimensions contains a condensate into which the AF state decays. Since the condensate is bosonic, this is a bosonic system of electrons, and so, insofar as we can see, must be superconducting. The behaviour of the gap, which is BCS-like, is consistent with our expectations.

Superconductivity co-exists with antiferromagnetism in the under-doped region.

We thank I. Hase, M. Hashimoto, S. Sharma, K. Yamaji, and all members of the Condensed Matter Physics group, AIST for extensive, informative and penetrating comments and discussions.

References

1. D. Dagotto, Rev. Mod. Phys. **66** (1994) 763;
   D. Scalapino, in K. S. Bedell, D. Coffey, D. E. Deltzer, D. Pines, J. R. Schrieffer (Eds.), 'High temperature superconductivity—the Los Alamos symposium—1989 Proceedings', Addison–Wesley Publishing Company, Redwood City, 1990, p. 314.
2. See, for example: H. Neuberger and T. Ziman, Phys. Rev. **B 39** (1989) 2608; H. Leutwyler, Phys. Rev. **D 49** (1994) 3033.
3. J. Bardeen, L. N. Cooper and J. R. Schrieffer, Phys. Rev. **108** (1957) 108.
4. A. A. Abrikosov, L. P. Gorkov and I. E. Dzyaloshinski, 'Methods of quantum field theory in statistical physics', Dover Publications, 1975.
5. V. N. Gribov, Eur. Phys. J. **C 10** (1999) 71 [arXiv:hep-ph/9807224]; ibid. **10** (1999) 91 [arXiv:hep-ph/9902279].
6. V. N. Gribov, Phys. Lett. **B 336** (1994) 243 [arXiv:hep-ph/9407269].
7. C. Kittel, 'Quantum Theory of Solids', John Wiley and Sons, 1963.
8. U.-J. Wiese and H.-P. Ying, Z. Physik **B 93** (1994) 147.
9. J. D. Bjorken and S. D. Drell, 'Relativistic Quantum Mechanics', McGraw–Hill, 1964.
10. 'Wolfram Mathematica online integrator', `http://integrals.wolfram.com/`.
11. 'Maxima, a Computer Algebra System', `http://maxima.sourceforge.net/`.
12. J. A. M. Vermaseren, arXiv:math-ph/0010025.
13. See, for example, the following and the references therein:
    M. Beneke, Phys. Rept. **317** (1999) 1 [arXiv:hep-ph/9807443];
    A. G. Grozin, arXiv:hep-ph/0311050.